

A dimension reduction approach to edge weight estimation for use in spatial models

Michael F. Christensen and Jo Eidsvik

July 4, 2024

Abstract

Models for areal data are traditionally defined using the neighborhood structure of the regions on which data are observed. The unweighted adjacency matrix of a graph is commonly used to characterize the relationships between locations, resulting in the implicit assumption that all pairs of neighboring regions interact similarly, an assumption which may not be true in practice. It has been shown that more complex spatial relationships between graph nodes may be represented when edge weights are allowed to vary. Christensen and Hoff [2024] introduced a covariance model for data observed on graphs which is more flexible than traditional alternatives, parameterizing covariance as a function of an unknown edge weights matrix. A potential issue with their approach is that each edge weight is treated as a unique parameter, resulting in increasingly challenging parameter estimation as graph size increases. Within this article we propose a framework for estimating edge weight matrices that reduces their effective dimension via a basis function representation of the edge weights. We show that this method may be used to enhance the performance and flexibility of covariance models parameterized by such matrices in a series of illustrations, simulations and data examples.

1 Introduction

Studies involving areal, or region indexed data are common in many settings including ecology [e.g. Hanks and Hooten, 2013], economics [e.g. Arbia, 2012], public health [e.g. Jin et al., 2005] and sociology [e.g. Garner and Raudenbush, 1991]. Models for spatially indexed data are typically defined such that observations close to one another in space exhibit higher correlation than

observations which are far apart. In contrast to spatial models for point-indexed data, which tend to characterize between-location dependence as a function of the geographic distances between observations, models for areal data generally define spatial dependence in terms of neighborhood or adjacency structure [Cressie, 1993].

The spatial structure of areal data may be represented using a graph, with each spatial region represented by a graph node and with edges existing between each pair of nodes corresponding to physically adjacent regions. First introduced by Besag [1974], the most commonly used spatial model for areal data is the conditional autoregressive (CAR) model. Given a graph $G = (V, E)$ having p nodes, we observe the random vector \mathbf{y} , where y_1, \dots, y_p are observations at each node of G . A CAR model defines a Markov random field where the conditional distribution of each element of \mathbf{y} is determined by the values of \mathbf{y} at adjacent nodes:

$$y_i | \mathbf{y}_{-i} \sim N \left(\sum_{j \sim i} \alpha w_{ij} y_j, \sigma^2 \right). \quad (1)$$

Equation 1 results in a marginal distribution for \mathbf{y} of

$$\mathbf{y} \sim N_p(\mathbf{0}, \sigma^2 (\mathbf{I}_p - \alpha \mathbf{W})^{-1}) \quad (2)$$

where $j \sim i$ indicates that node j is adjacent to node i , \mathbf{W} is a $p \times p$ adjacency or weights matrix (where $w_{ij} > 0$ if $j \sim i$ else $w_{ij} = 0$), $\sigma^2 > 0$ is a variance parameter, and α controls the degree of spatial correlation. In order to produce a valid covariance matrix, α must be bounded between the largest and smallest eigenvalue of \mathbf{W} [Ver Hoef et al., 2018]. An alternative form of the CAR model may be written

$$\mathbf{y} \sim N_p(\mathbf{0}, \sigma^2 (\text{diag}(\mathbf{W}\mathbf{1}_p) - \kappa \mathbf{W})^{-1}) \quad (3)$$

where $\text{diag}(\cdot)$ returns a diagonal matrix with entries equal to the input vector. This model is valid for all $|\kappa| < 1$. The intrinsic conditional autoregressive (ICAR) model is a special case of Equation 3 when $\kappa = 1$. This results in an improper distribution, but it may be reconfigured as a $p - 1$

dimensional distribution using the constraint $\sum y_i = 0$ [Besag and Kooperberg, 1995].

While many variants of the CAR and other similarly defined spatial autoregressive models have been developed and utilized, Ver Hoef et al. [2018] notes that in practice almost all such models have been implemented using the unweighted adjacency matrix of G , with $w_{ij} = 1$ if $i \sim j$, and $w_{ij} = 0$ otherwise. The CAR model is frequently used to characterize spatial random effects or an “error process” within a larger generalized linear model [Besag et al., 1991]; in many such contexts, interest in the covariance structure of the model has been secondary to inference on the fixed effects governing the model’s mean structure. However, the lack of a more complex weighting scheme results in a pattern of spatial dependence where the partial correlations between all pairs of adjacent regions are identical regardless of location within the overall spatial domain. Such models may be thought of as discrete space equivalents to stationary and isotropic covariance models for point indexed data in continuous space, properties which are frequently inappropriate for real world data [Guttorp et al., 1994].

Christensen and Hoff [2024] introduced a covariance model (which we will refer to as the graph deformation model or GDEF model within this article) for areal data exhibiting greater flexibility than the traditional CAR model. Given a graph $G = (V, E)$ with p nodes and random vector \mathbf{y} consisting of observations at each node of G , they define $\Sigma = \text{Cov}(\mathbf{y})$ as follows:

$$\begin{aligned}
 \Sigma_{ij} &= \sigma^2 \rho_v(d_{ij}) \\
 d_{ij} &= \sqrt{(\mathbf{e}_i - \mathbf{e}_j)^\top \{\mathbf{L}^+\}^2 (\mathbf{e}_i - \mathbf{e}_j)} \\
 \mathbf{L} &= \text{diag}(\mathbf{W}\mathbf{1}_p) - \mathbf{W} \\
 \sigma^2 &> 0, w_{ij} > 0 \text{ if } i \sim j, \text{ else } w_{ij} = 0, \text{ and } w_{ij} = w_{ji}.
 \end{aligned} \tag{4}$$

Here σ^2 is a scale parameter and $\rho_v(\cdot)$ is the Matérn correlation function [Matérn, 1960] with smoothness parameter v . The term d_{ij} may be thought of as the latent distance between nodes i and j and is defined as a function of unknown edge weights matrix \mathbf{W} . The matrix $\{\mathbf{L}^+\}^2 = \mathbf{L}^+\mathbf{L}^+$ is the square of the generalized inverse of the graph Laplacian \mathbf{L} , and $\{\mathbf{e}_i\}_{1:p}$ are the standard basis

vectors. The edge weights $\{w_{ij}\}_{i \sim j}$ are estimated from the observed data.

The GDEF model described in Equation 4 results in a valid covariance matrix for any combination of positive edge weights and the matrix \mathbf{W} is an identifiable parameter. While Christensen and Hoff [2024] demonstrate the flexibility and interpretive value of the GDEF approach, the authors also acknowledge that the model has limited scalability when applied to large graphs given the number of model parameters (each non-zero edge weight must be estimated individually) and computational intensity of the Markov chain Monte Carlo (MCMC) algorithm they used to obtain parameter estimates.

Both CAR and GDEF models are constructed using the edge weights matrix \mathbf{W} . While the GDEF model could be improved by coming up with a simpler and more efficient approach to estimation of \mathbf{W} , CAR models may be improved in practice by using a more complex approach. As noted, CAR models have traditionally been defined with \mathbf{W} equal to the unweighted adjacency matrix of the graphical representation of the spatial domain, a choice that is both simple and convenient but may be restrictive depending on the data and scientific question of interest. Despite likely under-utilization in practice, more complex weighting schemes for CAR models have been shown to be valuable, as in Hanks and Hooten [2013] and Ejigu and Wencheko [2020] which define edge weights using linear combinations of environmental covariates. Weighting schemes with even greater flexibility are also possible and potentially enable deeper understanding of the interaction between discretely observed spatial processes and the the spatial domain over which they are observed.

Within this article we introduce a new approach to estimating edge weights matrices that may be used within the GREF framework of Christensen and Hoff [2024] and which allows for the specification of CAR models that are considerably more flexible than existing variants. In the following section we provide a brief overview of necessary background information related to spatial basis functions, graphs, and spectral theory. In Section 3 we present our method and discuss some of its properties. Section 4 illustrates and evaluates the performance of our approach through

a series of simulation studies and a real data example. We conclude the article with a discussion of potential applications and extensions.

2 Background

Given a simple, undirected graph $G = (V, E)$, random variables $\{y_v : v \in V\}$ observed at the nodes V of G , and defining $\Sigma_{vv'} = \text{Cov}(y_v, y_{v'})$, we parameterize the covariance matrix as a function of \mathbf{W} , a matrix of unknown positive edge weights. We define \mathscr{W}_G to be the space of all edge weight matrices \mathbf{W} possible under G such that $w_{ij} > 0$ if an edge exists between nodes i and j and $w_{ij} = 0$ otherwise. As the number of nodes in G increases, so too does the size of \mathscr{W}_G . As such, setting a prior distribution for \mathbf{W} over the complete space \mathscr{W}_G (as in Christensen and Hoff [2024]) may not be feasible for graphs containing more than a few hundred nodes. To address this, we restrict the parameter space to $\mathbf{W} \in \mathscr{W}_G^B \subset \mathscr{W}_G$, where \mathscr{W}_G^B contains all possible edge weights matrices that can be obtained from a basis function representation (to be described in detail later) of the non-zero edge weights.

2.1 Basis functions and spatial models

If $y(\mathbf{s})$ is an observation of a random process at location $\mathbf{s} \in \mathscr{D}$ within some spatial domain (\mathscr{D} is typically a subset of \mathbb{R}^2 , but could also be the set of spatial regions under the areal data setting), with spatially indexed predictors $\mathbf{x}(\mathbf{s})$, a typical model for $y(\cdot)$ might be written as follows:

$$y(\mathbf{s}) = \mathbf{x}^\top(\mathbf{s})\boldsymbol{\beta} + u(\mathbf{s}) + \varepsilon(\mathbf{s}) \quad (5)$$

where $\boldsymbol{\beta}$ is a vector of coefficients, $u(\mathbf{s})$ is a spatial random effect and $\varepsilon(\mathbf{s}) \stackrel{iid}{\sim} N(0, \sigma^2)$ for all $\mathbf{s} \in \mathscr{D}$. Let $\mathbf{u} = (u(\mathbf{s}_1), \dots, u(\mathbf{s}_p))$ denote the vector of spatial random effects at some collection of p locations.

Instead of modeling $\mathbf{u} \sim N_p(\mathbf{0}, \Sigma)$ it is common to define $\mathbf{u} = \mathbf{M}\boldsymbol{\eta}$, where \mathbf{M} is an $p \times k$ matrix of $k \ll p$ basis functions, and $\boldsymbol{\eta} \sim N_k(\mathbf{0}, \Phi)$. Reduced-rank statistical models representing spatial random effects using basis functions are widespread. Examples of this include, but are not

limited to the kernel convolution approach [Higdon, 1998], predictive processes [Banerjee et al., 2008], spatial splines [Sangalli et al., 2013] the stochastic partial differential equation approach [Lindgren et al., 2011], and various eigenvector and principle component based methods [Hughes and Haran, 2013, Higdon et al., 2008, Lee and Haran, 2022]. Note that the majority of these methods were developed for point indexed data, though the framework of Hughes and Haran [2013] is designed specifically for areal data. Applying methods designed for one data type to another is possible, but requires assumptions that may not be appropriate in all settings [Gelfand et al., 2001].

Basis function methods tend to be very computationally efficient relative to full-rank Gaussian process models. Notably, some approaches to basis functions specification are also capable of addressing issues such as nonstationarity and anisotropy [Schmidt and Guttorp, 2020]. It has often been observed that methods based on low-rank representations of spatial random effects may result in oversmoothing as well as bias in the estimation of variance components [Stein, 2014, Datta et al., 2016, Banerjee et al., 2010]. Additionally, when pre-specifying the design matrix \mathbf{M} using some set of basis functions, the covariance of \mathbf{u} is restricted to matrices of the form $\mathbf{M}\Phi\mathbf{M}^\top$: in many instances, Φ is assumed to be a diagonal matrix or multiple of the identity matrix, resulting in strong and potentially inappropriate assumptions about model covariance structure. This may be especially true if analysis goals go beyond spatial prediction and smoothing and include inference regarding model covariance. Rather than modelling spatial random effects for areal data as a linear combination of basis functions, we propose using basis functions in a novel parameterization of edge weights matrix \mathbf{W} which is then incorporated into a CAR or GDEF model, resulting in a class of full-rank covariance matrices that are more flexible than traditional autoregressive models and less computationally demanding than the implementation of the GDEF used by Christensen and Hoff [2024].

2.2 Line graphs and an eigenvector basis

We now describe the basis used in this article. Given a graph $G = (V, E)$ having p nodes and q edges, one may define its line graph $L(G)$ as a graph with q nodes corresponding to each of the

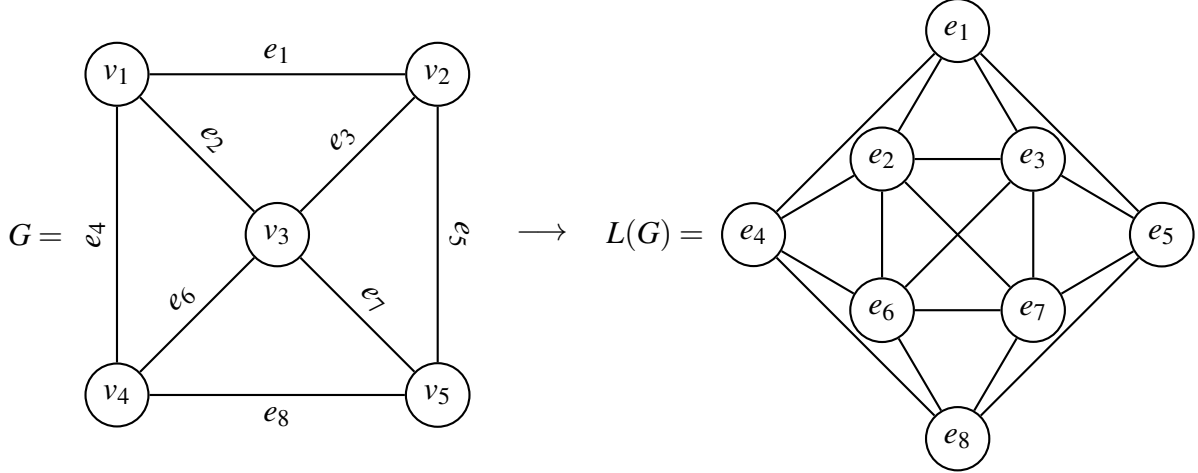


Figure 1: The graph G has corresponding line graph $L(G)$

edges of G , and edges between each pair of nodes corresponding to coincident edges in the original graph G . (Edges are considered coincident if they share a common node). Figure 1 illustrates the relationship between a graph G and its line graph $L(G)$ for a graph containing five nodes.

Let \mathbf{A}^L be the $q \times q$ adjacency matrix of $L(G)$, where $a_{ij}^L = 1$ if nodes i and j of $L(G)$ are adjacent and $a_{ij}^L = 0$ otherwise. Let $\mathbf{L}^L = \text{diag}(\mathbf{A}^L \mathbf{1}_q) - \mathbf{A}^L$ be the Laplacian matrix of $L(G)$. If $\mathbf{V}\mathbf{\Lambda}\mathbf{V}^\top$ is the eigendecomposition of \mathbf{L}^L , the columns vectors of \mathbf{V} form an orthonormal basis for \mathbb{R}^q . The eigenvalues of Laplacian matrices are non-negative and generally ordered from smallest to largest, with smallest non-zero eigenvalues corresponding to the most “important” eigenvectors. Laplacian matrices for connected graphs are positive-semidefinite and have exactly one eigenvalue (denoted λ_1) equal to 0 with corresponding eigenvector $\mathbf{v}_1 \propto \mathbf{1}$. Despite some referring to \mathbf{v}_1 as the “trivial” eigenvector, it has interpretive value as an intercept column within an eigenvector basis. Considerable work has been done in the field of spectral graph theory investigating the properties of the eigenvalues and eigenvectors of Laplacian matrices. See Spielman [2012] for greater detail on this topic.

To visualize the basis characterized by the eigendecomposition of the line graph Laplacian (LGL) Figure 2 depicts a selection of LGL eigenvectors for a 30×30 lattice graph, while Figure 3 depicts the LGL eigenvectors for the graph of the 100 counties of North Carolina (the spatial

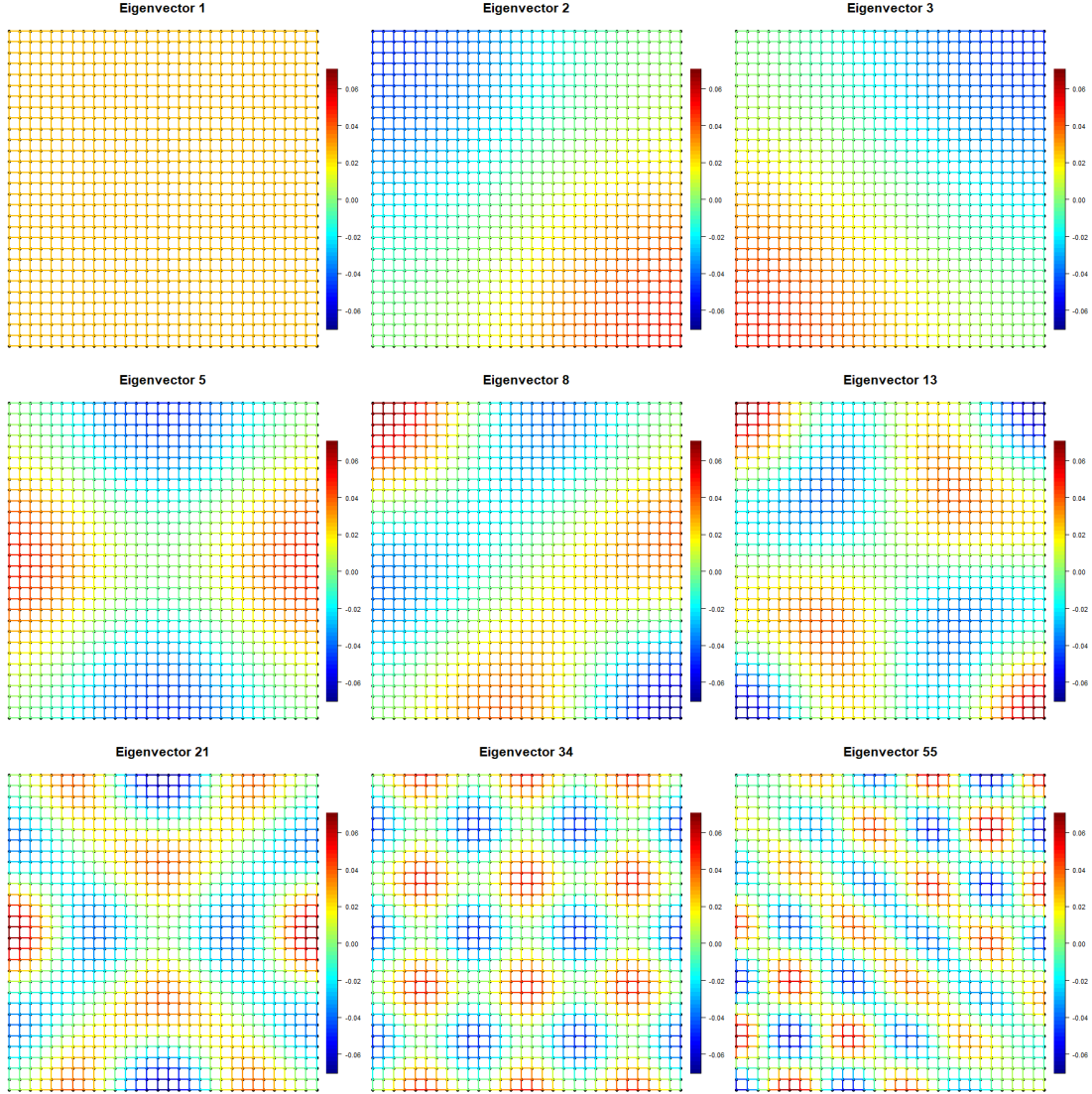


Figure 2: A selection of LGL eigenvectors for 30×30 lattice grid

domain analyzed in Christensen and Hoff [2024]). Note that each vector element corresponds to a specific edge of the original graph. We also highlight the harmonic behavior of these eigenvectors, with later eigenvectors exhibiting higher frequency oscillations between positively and negatively valued regions of the graph. This makes selection of the first k eigenvectors (corresponding to the k smallest eigenvalues) a natural choice of basis, with the “most important” initial eigenvectors capturing larger-scale trends in edge weight behavior and additional eigenvectors adding finer detail.

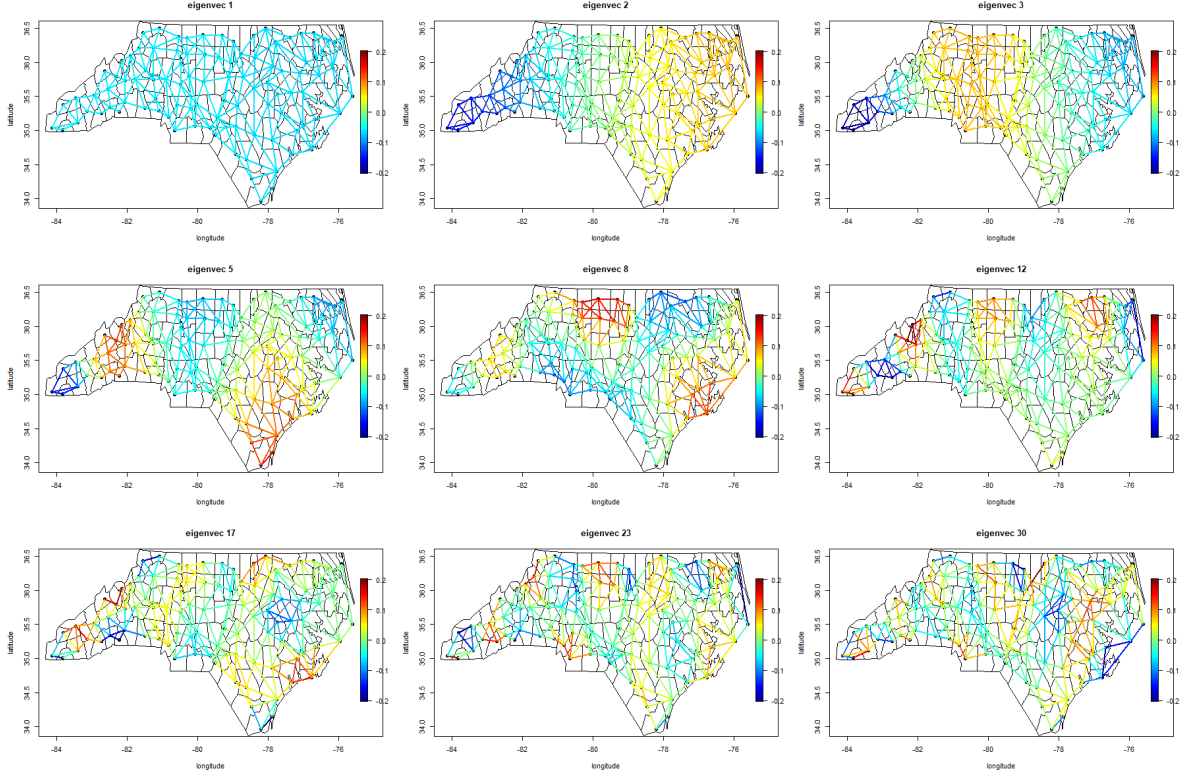


Figure 3: A selection of LGL eigenvectors for graph of the 100 counties of North Carolina

3 Method

Equations 3 and 4 describe two models for areal data, each parameterized by unknown edge weights matrix \mathbf{W} . Given a spatial domain representable by graph $G = (V, E)$ having p nodes and q edges, let \mathbf{w} be the q -length vector containing the unknown weights associated with the edges of G . The $p \times p$ edge weights matrix \mathbf{W} may be constructed from \mathbf{w} and vice versa. We construct the line graph $L(G)$ and obtain the line graph Laplacian \mathbf{L}^L , a $q \times q$ matrix. If $\mathbf{V}\mathbf{\Lambda}\mathbf{V}^\top = \mathbf{L}^L$ is the eigendecomposition of the LGL, let \mathbf{V}^k be the $q \times k$ matrix containing the k eigenvectors of \mathbf{L}^L associated with its k smallest eigenvalues. We can now represent \mathbf{w} as follows:

$$\mathbf{w} = \exp(\mathbf{V}^k \boldsymbol{\eta}), \boldsymbol{\eta} \in \mathbb{R}^k \quad (6)$$

Here, η is a k -length vector of basis coefficients that fully characterize the $p \times p$ edge weights matrix $\mathbf{W}(\eta)$. For all $\eta \in \mathbb{R}^k$, (and $\sigma^2 > 0$ and $|\kappa| < 1$) the CAR covariance matrix $\Sigma = \sigma^2(\text{diag}(\mathbf{W}(\eta)\mathbf{1}_p) - \kappa\mathbf{W}(\eta))^{-1}$ and the GDEF covariance matrix defined in Equation 4 are positive definite matrices. We now discuss some modeling considerations and illustrate properties of this method.

3.1 Contrasting the CAR and GDEF Approaches

We have stated that our framework for parameterizing the edge weights matrix of a given graph may be used when defining both CAR and GDEF models, but provided little discussion so far regarding the implications of using one covariance model or another. CAR models have sparse precision matrices, allowing for computationally efficient likelihood calculations. In contrast, the GDEF model specifies a dense covariance matrix; even when using the proposed basis function parameterization of \mathbf{W} , it is virtually impossible to use the GDEF covariance for graphs with over 10,000 nodes due to the impracticality of inverting matrices of that size. The computational advantages of the CAR approach do however come with trade-offs.

Several authors have noted that models which condition only on local or nearest-neighbor structure perform more poorly than those incorporating longer range dependencies [Gramacy and Apley, 2015, Katzfuss and Guinness, 2021, Guinness, 2018]. Realizations of spatial random fields produced by CAR models (including ICAR models, which induce perfect correlation between neighboring regions) are considerably less smooth than those generated by the GDEF model, a contrast that is more noticeable on graphs with a large number of nodes. Besag and Mondal [2005] shows that the standard ICAR model on a regular two-dimensional lattice grid converges asymptotically to the distribution of a two-dimensional Brownian motion as grid resolution increases, while Lindgren et al. [2011] shows that the ICAR model may be thought of as a discrete approximation to the limit of a Matérn random field whose range parameter goes to infinity and smoothness goes to zero. Paciorek [2013] demonstrates that CAR models using more than first order adjacency (extending graph structure to second order neighbors and beyond) do not result in meaningfully smoother fields. While computationally efficient, straightforward to implement and widely used,

CAR models carry implicit assumptions that may not be desirable in practice.

In contrast to the CAR model, the GDEF model accommodates a wider range of spatial dependence patterns for areal data. Equation 4 defines the GDEF covariance, where $\rho_\nu(\cdot)$ is the Matérn correlation function given below:

$$\rho_\nu(d) = \frac{2^{1-\nu}}{\Gamma(\nu)} \left(\sqrt{2\nu}d\right)^\nu K_\nu\left(\sqrt{2\nu}d\right). \quad (7)$$

Here d is the distance between two observations, $\nu > 0$ is a smoothness parameter, often fixed in practice, and K_ν is a modified Bessel function of the second kind of order ν . The exponential covariance function $\sigma^2 \exp(-d)$ is a special case of the Matérn covariance when $\nu = 1/2$; $\nu = 3/2$ and $\nu = 5/2$ are popular choices for spatial models, and the squared exponential covariance $\sigma^2 \exp(-d^2/2)$ is the limit of Equation 7 as ν goes to infinity. Those familiar with the Matérn family of covariance functions may note that Equation 7 omits an explicit range parameter. As discussed in Christensen and Hoff [2024], the range parameter of the GDEF model is implicitly defined by the scale of the edge weights matrix, e.g. multiplying \mathbf{W} by a factor of two is equivalent to doubling the range parameter, a property we now illustrate.

Figure 4 highlights some distinctions between the CAR and GDEF approaches. Depicted samples were generated over a 30×30 grid from a mean zero normal distribution. Each row corresponds to a different covariance model: the CAR model from Equation 3 with $\kappa = 0.95$, the ICAR model with a sum-to-zero constraint (the “smoothest” possible CAR model) and the GDEF model with four different values of ν . In the first column, \mathbf{W} was constructed such that $w_{ij} = 4$ for all $i \sim j$, with different constants used in subsequent columns. Across all settings the scale parameter σ^2 was set equal to 1. As expected, samples produced by the CAR models and the GDEF model for $\nu = 1/2$ are visibly less smooth than those from GDEF models with larger values of ν . The impact that the scale of \mathbf{W} has on each model is also notable. As previous stated, the scale of \mathbf{W} may thought of as the implicit range parameter within the GDEF; samples with edge weights equal to 4 exhibit slower decay in spatial correlation than those with smaller edge weights. For CAR

models, the scale of \mathbf{W} doesn't influence range, but rather the scale of marginal variances. (From Equation 3, it is clear multiplying \mathbf{W} by some constant is equivalent to dividing σ^2 by that same constant, indicating that the CAR model as we have defined it is over parameterized, which we address later.)

The notion of range within CAR models is trickier to characterize than for GDEF models. While the correlation parameter κ ostensibly controls the smoothness of the Markov random field and the rate of spatial decay between areal regions, it is highly sensitive to the resolution of the spatial domain. This may be particularly relevant when the CAR model is viewed as the discretization of some continuous spatial process. As areal resolution becomes finer, the space of region-averaged continuous spatial processes that could be represented using a CAR or ICAR model shrinks. Figure 5 highlights this, which depicts samples from an ICAR model at different spatial resolutions. If each grid represents the same subset of \mathbb{R}^2 and samples are viewed as the region-averaged realizations of continuous spatial processes, samples over coarser grids could correspond to smoother underlying processes than those generated at higher resolutions. In general we find that the GDEF model can be used to represent a wider range of spatial dependence patterns, and is less sensitive to how areal units are defined, though there are practical settings in which the computational efficiency of the CAR model may trump these considerations.

3.2 Impact and interpretation of basis coefficients

The illustrations in Figures 4 and 5 depict samples from distributions defined by uniform edge weights, but a major aim of this article is to show how flexibly defining the edge weights matrix \mathbf{W} can lead to more complex and potentially useful covariance structures. As discussed in Christensen and Hoff [2024] regarding the GDEF model, each possible edge weights matrix \mathbf{W} corresponds to an embedding of the graph in high-dimensional Euclidean space which is unique up to isometry. The distances between nodes in this embedding may be thought of as the “intrinsic” distances between regions. The GDEF model may be viewed as the graph equivalent of the spatial deformation approach for modeling nonstationary data defined by Sampson and Guttorp [1992], where

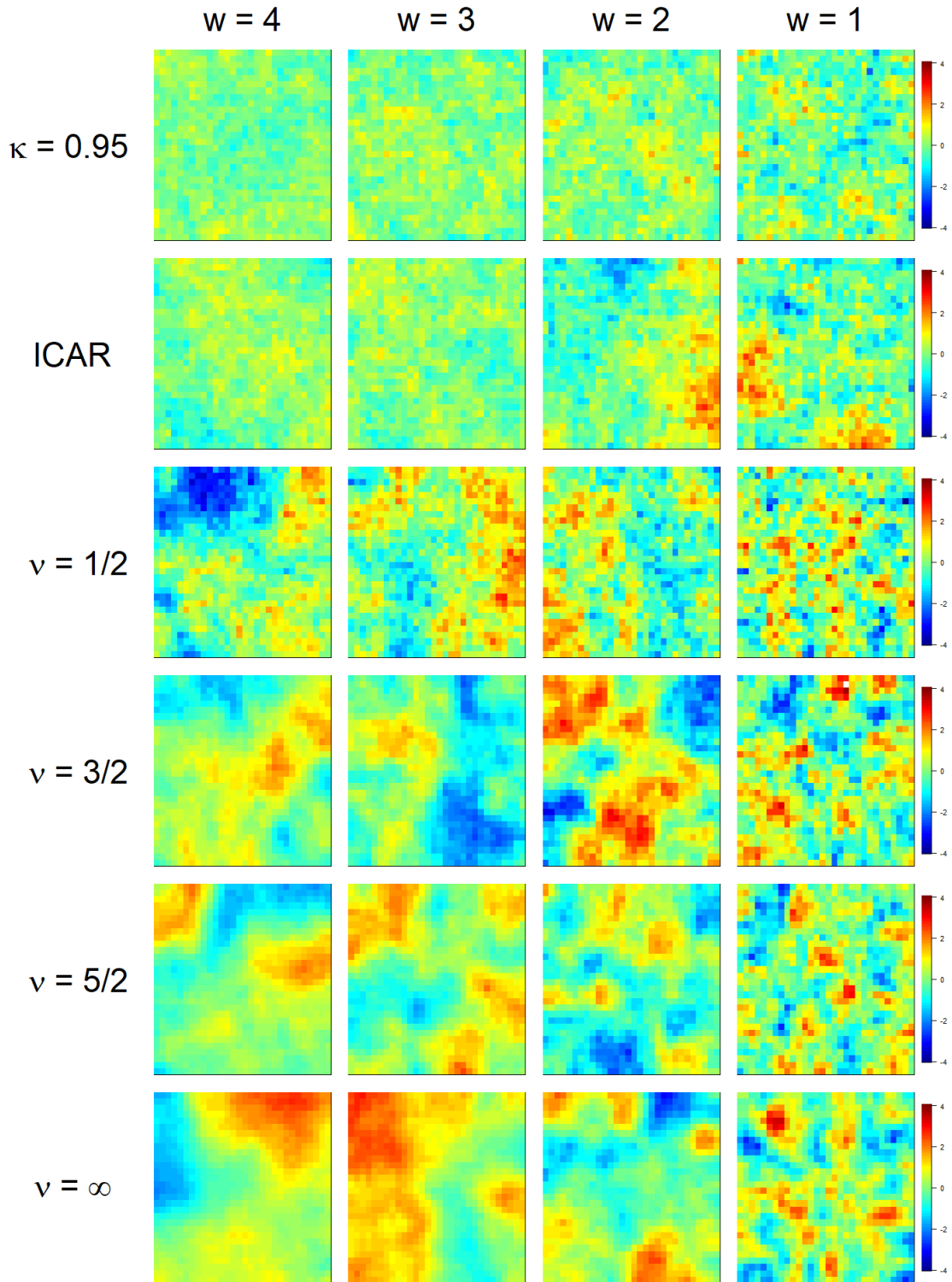


Figure 4: Samples from $N(\mathbf{0}, \Sigma)$ over a 30×30 grid with uniform edge weights. Columns correspond to the weight of all nonzero entries in \mathbf{W} , while each row corresponds to a different parameterization of Σ . The first row uses the CAR covariance with $\kappa = 0.9$, the second uses the ICAR covariance, and subsequent rows use the GDEF covariance for different values of ν .

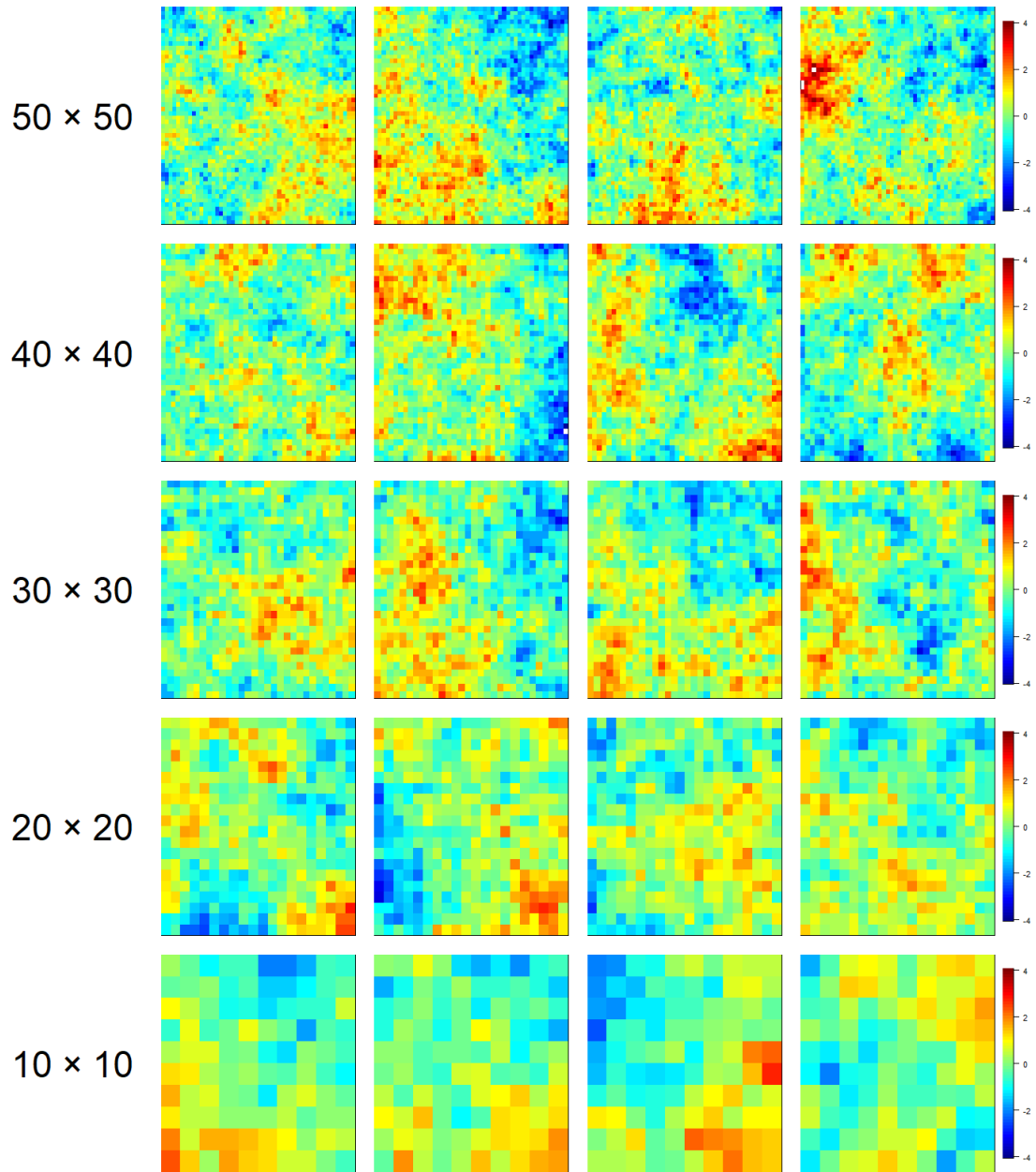


Figure 5: Samples from an ICAR model with uniform edge weights at different grid resolutions.

the deformation function is estimated by placing a prior on the edge weights. This interpretation leads us to say that nodes in regions containing high valued edges are “closer” to each other than regions with low valued edges. While the CAR model does not directly admit a distance based interpretation of \mathbf{W} , it can be said of both the CAR and GDEF approaches that edges with large weights correspond to greater connectivity between incident nodes.

Let $\mathbf{W}(\boldsymbol{\eta})$ be the $p \times p$ matrix of edge weights parameterized by $\boldsymbol{\eta} \in \mathbb{R}^k$. Equation 6 states that the log of the q -length vector containing the unique edge weights in $\mathbf{W}(\boldsymbol{\eta})$ is a linear combination of a collection of k basis functions of length q , with \mathbf{V}^k defined as the eigenvectors of the line graph Laplacian corresponding to the k smallest eigenvectors. We wish to provide some insight into the interpretation of the coefficient vector $\boldsymbol{\eta} = (\eta_1, \dots, \eta_k)'$ and illustrate some of the covariance patterns this construction can produce.

As previously noted, the first eigenvector of our basis, \mathbf{v}_1^k is always constant. This means that $\eta_1 \mathbf{v}_1^k$ is constant and may be viewed as the intercept for the log edge weights. Because $\exp(\mathbf{V}^k \boldsymbol{\eta}) = \exp(\eta_1 \mathbf{v}_1^k) \odot \exp(\mathbf{V}_{-1}^k \boldsymbol{\eta}_{-1})$, the vector $\exp(\eta_1 \mathbf{v}_1^k)$ may be viewed as a scaling factor for the edge weights matrix $\mathbf{W}(\boldsymbol{\eta}_{-1})$ which is defined using the other $k - 1$ basis functions. In the GDEF model, this scaling factor is directly related to the range of spatial correlation, while in the CAR model, the scaling factor is redundant when σ^2 is estimated. As such, we recommend fixing $\eta_1 = 0$ when using the basis function approach to characterizing the edge weights matrix for CAR models. Subsequent coefficients in $\boldsymbol{\eta}$ may be interpreted in context of the eigenvectors with which they are associated. As depicted in Figure 2, the second LGL eigenvector of a 30×30 grid characterizes a contrast between the upper left and lower right corners of the spatial domain. Figure 6 depicts samples from different covariance models defined using only the first two LGL eigenvectors. Across covariance models it can be seen how observations in one corner of the spatial domain are highly correlated, while the effective range of spatial correlation is much smaller in the opposite corner. Spatial covariance patterns such as this do appear in real world settings. Paciorek and Schervish [2006] presents a data set for precipitation in Colorado in which obser-

vations east of the Rocky mountains are highly correlated over long distances, whereas spatial correlations between observations in the mountainous western half of the state decay rapidly over short distances.

Different linear combinations of basis functions can produce a wide array of covariance structures. Figure 7 depicts a linear combination of four eigenvectors that results in covariance where observations at the borders of the spatial domain are highly correlated, while observations in the interior are not. In effect locations at opposite corners of the grid are “closer” together than locations that are both near the center. The more basis functions are included, the more flexible the covariance, though there are generally diminishing returns as the number of eigenvectors used increases due to the higher spatial frequencies exhibited by later eigenvectors. Omitting these high frequency eigenvectors essentially assumes that the edge weights themselves exhibit some degree of spatial smoothness. Intuition on how to select the number of basis functions is provided later in this article.

3.3 Incorporating covariates

We may be interested in the question of whether certain environmental features inhibit or facilitate connectivity between regions in our spatial domain. As such we may wish to model edge weights as a function of environmental covariates. Generally speaking, we will not have covariates that are explicitly associated with the edges of our graph. If \mathbf{X} is a $p \times r$ matrix containing r features for each of the p nodes in a graph, Hanks and Hooten [2013] suggested defining \mathbf{X}^E , a $q \times r$ feature matrix for the graph’s edges, by averaging the features of adjacent nodes:

$$\mathbf{x}^{e_{ij}} = \frac{\mathbf{x}_i + \mathbf{x}_j}{2}. \quad (8)$$

Here $\mathbf{x}^{e_{ij}}$ is the row of \mathbf{X}^E corresponding to the edge linking nodes i and j . The matrix \mathbf{X}^E could also be constructed treating differences in the features of adjacent regions as a covariate itself. Others have suggested that the length of the shared border between two adjacent regions may be

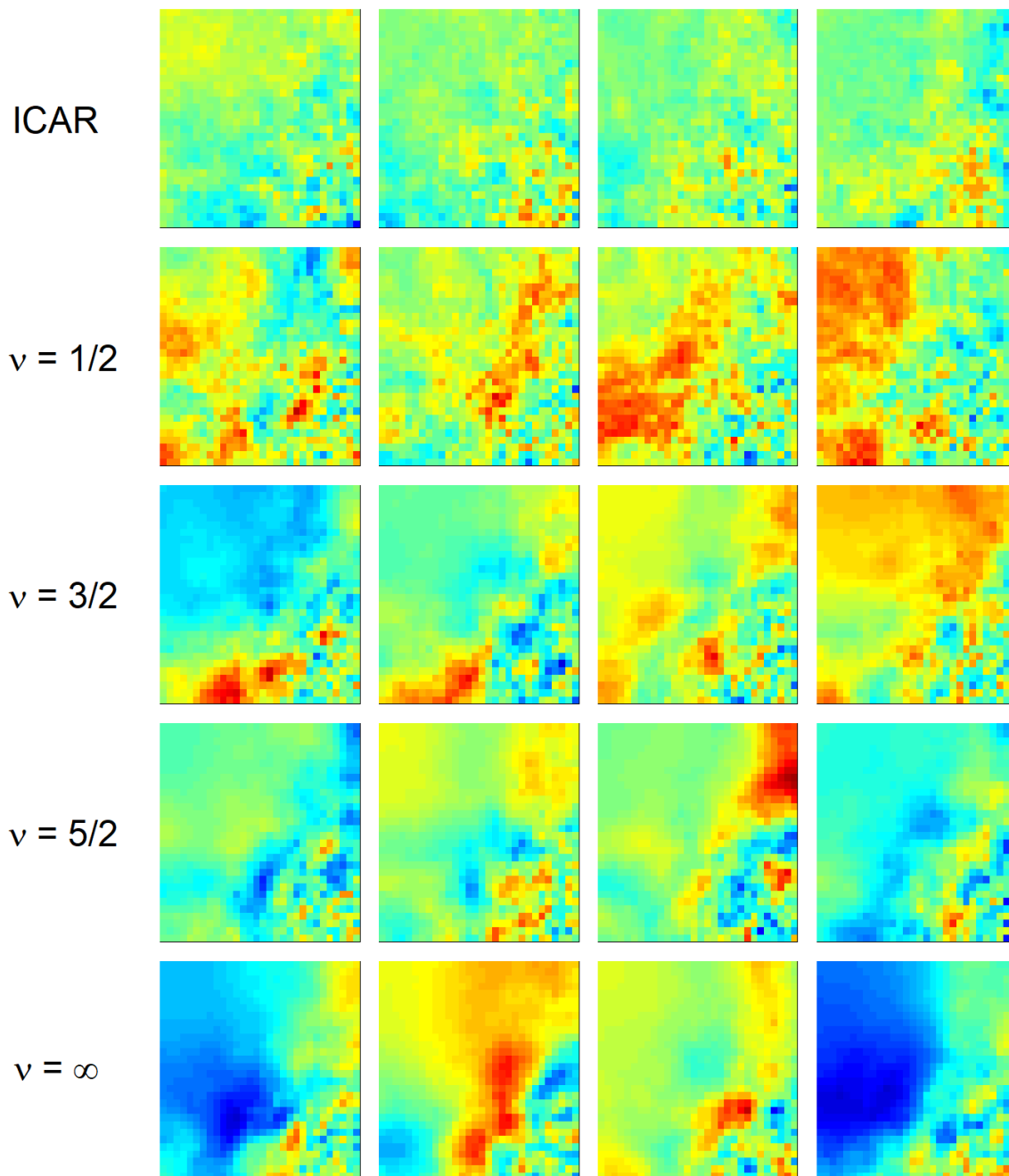


Figure 6: Samples from $N(\mathbf{0}, \Sigma)$ over a 30×30 grid using two basis functions with $\eta_1 = \eta_2 = 50$. Note how spatial correlation decays at different rates across the spatial domain.

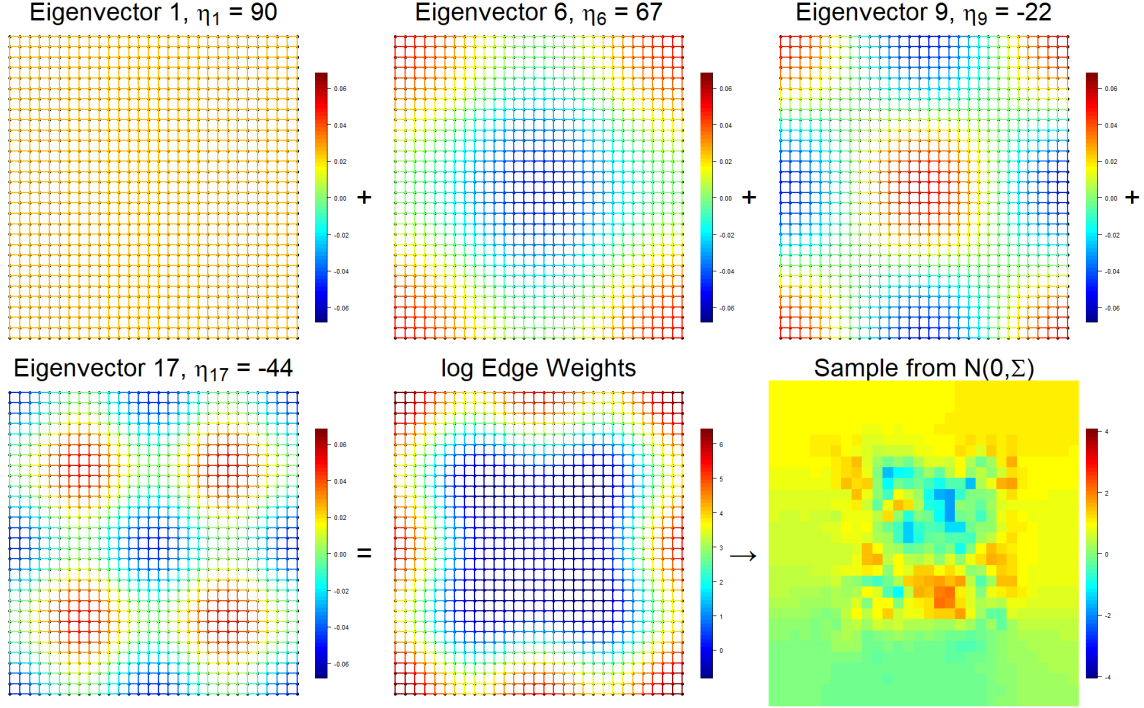


Figure 7: Illustration of how limited number of basis functions may combine to produce complex covariance structures. Σ defined using double exponential covariance.

important to consider. However \mathbf{X}^E is defined, we can augment the basis function model for edge weights in Equation 6 by setting

$$\mathbf{w} = \exp(\mathbf{X}^E \boldsymbol{\psi} + \mathbf{V}^k \boldsymbol{\eta}), \quad \boldsymbol{\psi} \in \mathbb{R}^r, \quad \boldsymbol{\eta} \in \mathbb{R}^k. \quad (9)$$

In order to avoid confounding between $\boldsymbol{\psi}$ and $\boldsymbol{\eta}$ due to correlation between \mathbf{X}^E and \mathbf{V}^k , let \mathbf{V}^\perp contain the eigenvectors of $\mathbf{X}^\perp \mathbf{L}^L \mathbf{X}^\perp$, where $\mathbf{X}^\perp = (\mathbf{I}_q - \mathbf{X}^E (\mathbf{X}^{E\top} \mathbf{X}^E)^{-1} \mathbf{X}^{E\top})$ is the projection onto the orthogonal complement of the column space of \mathbf{X}^E . The $q \times k$ matrix $\mathbf{V}^{k\perp}$ contains the k eigenvectors corresponding to the smallest eigenvalues of $\mathbf{X}^\perp \mathbf{L}^L \mathbf{X}^\perp$. The matrix \mathbf{X}^E is orthogonal to $\mathbf{V}^{k\perp}$, which may improve estimation and interpretation of $\boldsymbol{\psi}$. This approach to spatial deconfounding was introduced by Reich et al. [2006] and has seen widespread use since then, though there is debate as to whether such adjustments are appropriate [Zimmerman and Ver Hoef, 2022]. While we have little to contribute to this discussion from a theoretical perspective, we find that

using the orthogonalized $\mathbf{V}^{k\perp}$ results in a slightly more flexible covariance model when weights are defined using Equation 9.

3.4 Parameter estimation and model fitting

Given graph $G = (V, E)$ with p nodes and q edges, we make repeated observations of the collection of random variables $\{y_v : v \in V\}$; each repetition is recorded as $\mathbf{y}_i \in \mathbb{R}^p$ for $i \in 1, \dots, n$. These observations may be stored in the $n \times p$ data matrix \mathbf{Y} , where y_{ij} is the i th observation at the j th node of G . For now, we assume that $\mathbf{y}_i \stackrel{iid}{\sim} N_p(\mathbf{0}, \Sigma)$, with Σ parameterized by $\theta = (\sigma^2, \eta)$ for the GDEF model and $\theta = (\sigma^2, \eta, \kappa)$ for the CAR model. Christensen and Hoff [2024] only considered settings with multiple observations of the spatial process. This was necessary due each edge weight being a unique parameter and the fact $q > p$ in almost all settings. The dimension reduction of the basis function approach to estimation of \mathbf{W} allows us to model the covariance of spatial processes with only a single realization ($n = 1$).

The maximum likelihood estimator (MLE) for θ may be obtained using the Newton-Raphson algorithm which requires computation of the first and second derivatives of the log likelihood $\ell(\theta; \mathbf{Y})$ with respect to θ . Details on the form of $\nabla_{\ell}(\theta) = \frac{\partial \ell(\theta; \mathbf{Y})}{\partial \theta}$ and $\mathbf{H}_{\ell}(\theta) = \frac{\partial^2 \ell(\theta; \mathbf{Y})}{\partial \theta^2}$ for the models discussed in this article are provided in Appendix 2. Given data \mathbf{Y} and an initial set of parameter values θ^0 we can maximize the likelihood by iteratively calculating

$$\theta^l = \theta^{l-1} - \gamma \mathbb{E} \left[\mathbf{H}_{\ell}(\theta^{l-1}) \right]^{-1} \left(\nabla_{\ell}(\theta^{l-1}) \right) \quad (10)$$

until θ^l converges to the MLE. Here γ is a scaling parameter between 0 and 1. Smaller γ provides more robust optimization, while $\gamma = 1$ will generally be faster.

Uncertainty quantification may be conducted using the approximation

$$\hat{\theta} \sim N \left(\theta, - \left[\mathbf{H}_{\ell}(\hat{\theta}) \right]^{-1} \right). \quad (11)$$

Note when employing the Newton-Raphson algorithm in Equation 10 that we use the expectation

of the Hessian matrix $\mathbf{H}_\ell(\boldsymbol{\theta})$, which is less computationally intensive to obtain than the Hessian matrix itself. We only need to compute $\mathbf{H}_\ell(\boldsymbol{\theta})$ once after obtaining the MLE in order to use the approximation in Equation 11.

We have also used Bayesian estimation techniques to fit the model described in this article. Details on recommend prior choices and MCMC algorithms are also provided in Appendix 2.

4 Illustrations

Within this section we evaluate the performance of our approach under a variety of settings and in comparison to alternative methods. We consider both simulated and real-world data examples.

4.1 Simulations

We begin with three simulation studies. In the first we evaluate approximate confidence interval coverage rates when the model is correctly specified. In the second, we consider how to select the number of basis functions when implementing our method. The third simulation assesses model performance under misspecification, evaluating the Kullback-Leibler divergence between the true data generating distribution and the estimated distribution.

Sim 1: Approximate confidence interval coverage

We defined 10×10 and 20×20 lattices, and obtained the LGL eigenvectors for each. We selected k eigenvectors and simulated $\boldsymbol{\eta} \sim N_k(\mathbf{0}, \boldsymbol{\Phi})$, where $\boldsymbol{\Phi}$ is a diagonal matrix with first entry (corresponding to the variance of the “intercept” eigenvector) equal to 0.5 and all other diagonal entries equal to 25. We then generated n samples from $N_p(\mathbf{0}, \boldsymbol{\Sigma}(\boldsymbol{\eta}))$ where $\boldsymbol{\Sigma}(\boldsymbol{\eta})$ is defined by Equations 4 and 6, using a Matérn covariance with $\nu = 3/2$ and fixing $\sigma^2 = 1$. This was done for each of $k \in \{10, 30\}$ and $n \in \{1, 10, 50\}$. We obtained the MLE $\hat{\boldsymbol{\eta}}$ and calculated approximate 90% confidence intervals for $\boldsymbol{\eta}$ using Fisher’s approximation. The simulation was repeated ten times, with coverage rates provided in Table 1.

In general coverage rates are appropriate, the exception being under the settings $k = 30$ and

| | $n = 1$ | $n = 10$ | $n = 50$ |
|-------------------|-----------------------|-----------------------|-----------------------|
| $p = 100, k = 10$ | 0.880 (± 0.039) | 0.910 (± 0.023) | 0.870 (± 0.040) |
| $p = 100, k = 30$ | 0.804 (± 0.040) | 0.867 (± 0.027) | 0.927 (± 0.015) |
| $p = 400, k = 10$ | 0.920 (± 0.025) | 0.910 (± 0.023) | 0.910 (± 0.031) |
| $p = 400, k = 30$ | 0.907 (± 0.018) | 0.900 (± 0.021) | 0.883 (± 0.019) |

Table 1: Coverage rates of approximate 90% confidence intervals. Monte Carlo standard error in parentheses.

$n = 1$ over a 10×10 lattice. On top of having lower than expected coverage, Newton’s method diverged in one of the ten simulations under these settings, indicating that one observation of a spatial process over a graph with $p = 100$ nodes may not be enough to inform the estimation of Σ using $k = 30$ basis functions. In general however, we feel that inference based on Fisher’s approximation to the distribution of the MLE is appropriate. We investigate choice of k in the following simulation.

Sim 2: Number of basis functions

Once again, we defined 10×10 and 20×20 lattices obtaining LGL eigenvectors for each. Instead of simulating edge weights directly from Equation 6 we generate an edge weights matrix \mathbf{W} from an ICAR model using the line graph adjacency matrix to define the associations between edges. Figure 8 depicts sampled edge weights over a 20×20 lattice. The spatial dependence in the simulated edge weights themselves means that \mathbf{W} can be well approximated using our method. Larger numbers of basis functions will improve this approximation, but at the cost of model complexity and potential computational instability. The simulated \mathbf{W} was used to define a covariance matrix according to Equation 4 with $\nu = 3/2$ and $\sigma^2 = 1$. Independent samples were generated from $N_p(\mathbf{0}, \Sigma)$ and stored in $n \times p$ matrix \mathbf{Y} for $n \in \{1, 10, 50\}$. For each simulated \mathbf{Y} we fit a GDEF model using Matérn covariance with $\nu = 3/2$ using $k \in \{10, 20, \dots, 100\}$ basis functions and evaluated AIC and BIC for each of the 10 model fits, with lower values of

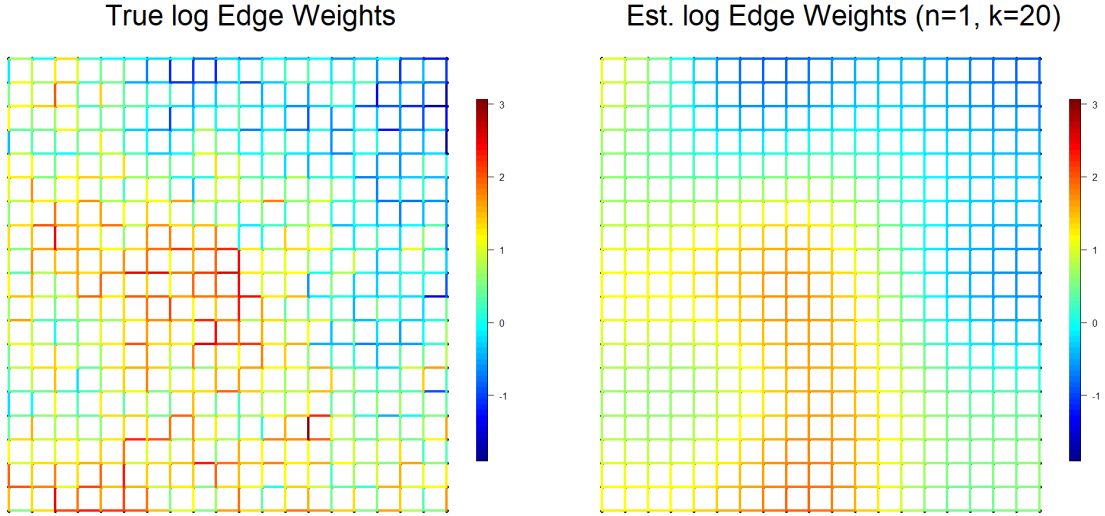


Figure 8: Simulated \mathbf{W} on left, with $\hat{\mathbf{W}}$ on right (estimated from $n = 1$ observations and using $k = 20$ basis functions). Approximation “smooths” the true edge weights.

$$\text{AIC} = -2\ell(\boldsymbol{\eta}; \mathbf{Y}) + 2k \tag{12}$$

$$\text{BIC} = -2\ell(\boldsymbol{\eta}; \mathbf{Y}) + k \log(np)$$

begin selected. The simulation was repeated 10 times. Table 2 contains information regarding the AIC- and BIC-preferred choices of k .

| | Mode k (AIC) | Mean k (AIC) | Mode k (BIC) | Mean k (BIC) |
|-------------------|----------------|----------------|----------------|----------------|
| $p = 100, n = 1$ | 10 | 12 | 10 | 10 |
| $p = 100, n = 10$ | 40 | 58 | 10 | 11 |
| $p = 100, n = 50$ | 100 | 100 | 40 | 42 |
| $p = 400, n = 1$ | 20 | 37 | 10 | 10 |
| $p = 400, n = 10$ | 100 | 99 | 30 | 39 |
| $p = 400, n = 50$ | 100 | 100 | 100 | 99 |

Table 2: Mode k indicates the most commonly selected number of basis functions, while Mean k indicates the average number of selected basis functions. Larger grids and larger sample sizes result in preference for higher k .

Across simulation settings, we see that models with higher k perform better on the larger grid and with bigger sample sizes. This is unsurprising as larger amounts of data should be expected to support more complicated models. AIC and BIC are considered not because they are objectively

the best tools for model selection, but because they provide a likelihood-based starting point for the question of how to choose the number of eigenvectors when implementing our method. BIC is more conservative than AIC due to a larger model size penalty. The two criteria also differ in that AIC is calibrated for improving predictive accuracy, while BIC may be viewed as favoring the model that best approximates the marginal distribution of the data [Gelman et al., 2014]. The fact that the two criteria frequently prefer different values of k provides some intuition for the range on model size that may be appropriate. Using the information in Table 2, a reasonable starting point is to select $k = \sqrt{np}$ when the model reasonably approximates the true data generating process, as was the case within this simulation. Optimal choice of k will also be contingent on the nature of the spatial process itself, as evidence of more complicated patterns of spatial dependence may indicate that larger numbers of basis functions should be used. Table 3 contains the rates at which the Newton-Raphson algorithm used to estimate $\hat{\eta}$ failed to converge across different simulation settings, with the majority of instances occurring for large k and $n = 1$. When computational instability is encountered, refitting with smaller k will frequently resolve the issue; the possibility of instability due to significant model misspecification should however be considered.

| | $k = 40$ | $k = 50$ | $k = 60$ | $k = 70$ | $k = 80$ | $k = 90$ | $k = 100$ |
|-------------------|----------|----------|----------|----------|----------|----------|-----------|
| $p = 100, n = 1$ | 0.3 | 0.7 | 0.8 | 1.0 | 1.0 | 1.0 | 1.0 |
| $p = 100, n = 10$ | 0.0 | 0.0 | 0.0 | 0.0 | 0.0 | 0.2 | 0.1 |
| $p = 100, n = 50$ | 0.0 | 0.0 | 0.0 | 0.0 | 0.0 | 0.0 | 0.0 |

Table 3: Frequency with which Newton-Raphson algorithm failed to converge. Estimation was stable for all $k < 40$ and for all settings over the 20×20 lattice.

Sim 3: Model performance under misspecification

The previous simulation evaluated the performance of the GDEF model for different values of k when the true data generating process was a GDEF model with an edge weights matrix from outside of the parameter space characterized by Equation 6. We now consider the performance of the GDEF model when data comes from a distinct nonstationary covariance model. Given a nonstationary spatial process $Z(\mathbf{s})$ observed at $\mathbf{s} \in \mathbb{R}^2$ the spatial deformation approach of Sampson

and Guttorp [1992] defines the process' covariance such that

$$\text{Cov}(Z(\mathbf{s}, \mathbf{s}')) = \sigma^2 \rho(\|g(\mathbf{s}) - g(\mathbf{s}')\|) \quad (13)$$

where $g(\cdot)$ is a transformation from the geographic location \mathbf{s} to its location $g(\mathbf{s})$ in a “deformed” space wherein covariance is stationary and isotropic.

Inspired by this approach, we simulate data by first defining a 15×15 lattice. We then deform the grid by randomly selecting ten “deformation points” $d_{1:10} \in (1, 15)^2$ before sequentially shrinking or expanding the grid towards or away from these locations, as illustrated by Figure 9. Let \mathbf{D}^D be the 225×225 matrix of Euclidean distances between the nodes of the deformed lattice. Applying a Matérn correlation function to \mathbf{D}^D results in a covariance matrix that is nonstationary with respect to \mathbf{D} , the matrix of Euclidean distances between the original grid point locations. We generate n observations from the following model

$$\begin{aligned} \mathbf{y}_i &= \beta_0 \mathbf{1} + \mathbf{z}_i + \varepsilon_i \\ \mathbf{z}_i &\sim N_p(\mathbf{0}, \sigma^2 \Phi) \\ \varepsilon_i &\sim N_p(\mathbf{0}, \tau^2 \mathbf{I}_p) \end{aligned} \quad (14)$$

where \mathbf{z}_i is a vector of spatial random effects with covariance matrix Φ defined using a Matérn correlation function with smoothness $\nu = 5/2$

$$\Phi = \left(1 + \frac{\sqrt{5}}{\rho} \mathbf{D}^D + \frac{5}{3\rho^2} \{\mathbf{D}^D\}^{\circ 2} \right) \odot \exp\left(\frac{\sqrt{5}}{\rho} \mathbf{D}^D \right) \quad (15)$$

We set $\beta_0 = 0$, $\sigma^2 = 0.9$, $\tau^2 = 0.1$, $\rho = 3$. We fit the GDEF and other models to the simulated \mathbf{Y} as illustrated by Figure 10, which depicts a deformed lattice, samples of \mathbf{y}_i produced by that deformation, and an estimated edge weights matrix.

We randomly generated 125 unique grid deformations. For each deformation we sampled \mathbf{Y} as described above for $n \in \{1, 2, 3, 5, 10, 25, 50\}$ and fit Equation 14 while defining the covariance

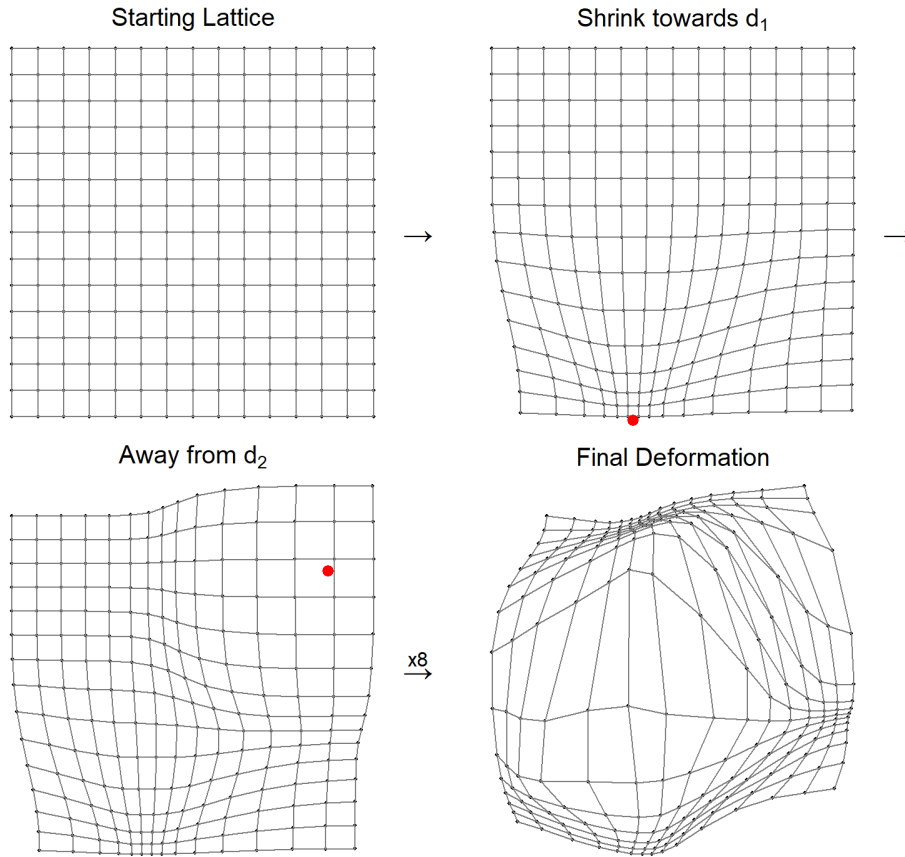


Figure 9: Deformed lattice obtained by repeatedly expanding and contracting grid around random locations. Each simulation replicate used a uniquely generated deformation.

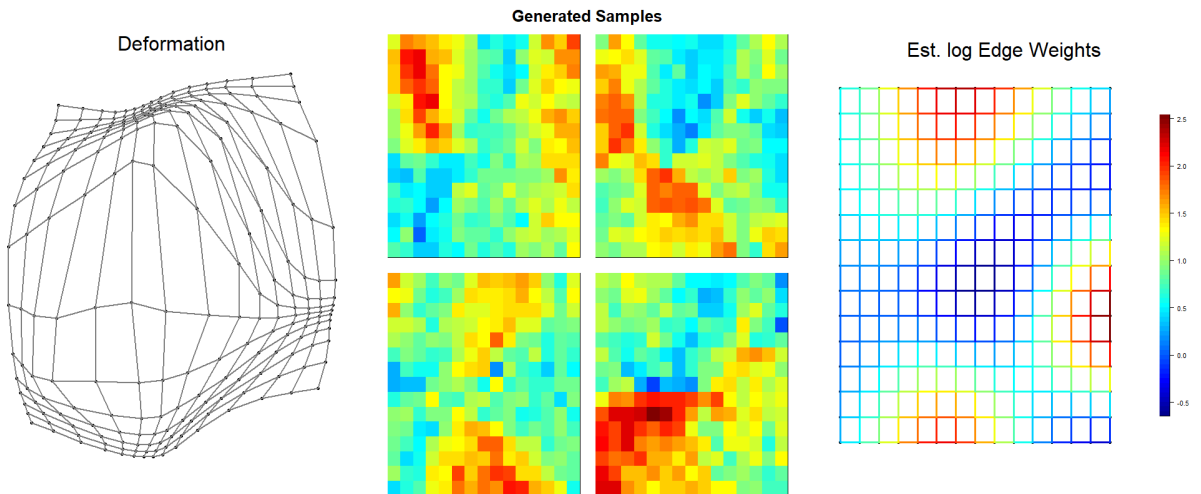


Figure 10: Distances between deformed grid locations define a nonstationary covariance matrix Σ . Data \mathbf{Y} generated from $N_p(\mathbf{0}, \Sigma)$. GDEF model is fit to \mathbf{Y} , producing the depicted $\hat{\mathbf{W}}$ and corresponding $\hat{\Sigma}^{GDEF}$.

of the random effects \mathbf{z}_i using the following six submodels: a GDEF model with $\nu = 3/2$ and $k = 15$ basis functions, a GDEF model using the double exponential covariance function ($\nu = \infty$) and $k = 15$ basis functions, the spatial deformation approach of Sampson and Guttorp [1992] (S&G) as implemented by the `deform` R package [Youngman, 2023], a simple Matérn covariance model with $\nu = 5/2$ and using the Euclidean distances between non-deformed lattice nodes, the method presented in Hughes and Haran [2013] (H&H) for modeling random effects in areal data using 100 basis functions, and a standard CAR model using an unweighted adjacency matrix. The spatial deformation approach and the stationary Matérn covariance model treat the data as though it were point-indexed, while all other approaches utilize only the lattice’s graphical structure; note however, that the true data generating process exists in continuous space.

Let $\Sigma = \sigma^2\Phi + \tau^2\mathbf{I}_p$ be the marginal covariance of \mathbf{y}_i integrated over the random effects \mathbf{z}_i . For each \mathbf{Y} and fitted model, we obtain the MLE $\hat{\Sigma}$ and compute $\text{KL}(N_p(\mathbf{0}, \Sigma), N_p(\mathbf{0}, \hat{\Sigma}))$, the Kullback-Leibler (KL) divergence between the true data generating distribution and the distribution characterized by the estimated covariance. As both distributions are mean-zero and Gaussian, KL divergence may be computed using only the covariance matrices Σ and $\hat{\Sigma}$:

$$\text{KL}(\Sigma, \hat{\Sigma}) = \frac{1}{2} \left(\log \frac{|\hat{\Sigma}|}{|\Sigma|} + \text{tr}(\hat{\Sigma}^{-1}\Sigma) - p \right) \quad (16)$$

Table 4 depicts the average KL divergence between the true distributions and the distributions estimated by the six models. Note that the true distribution is different for each of the 125 replicates which used a unique deformation. We also consider the frequency with which each model had the smallest KL divergence under the same settings. As can be seen, the GDEF model (for both choices of ν) performs well across sample sizes, with the simple Matérn model for $n = 1$ being the only alternative that was frequently competitive in this simulation. While potentially surprising that the simple Matérn covariance model using the non-deformed distances outclasses many of the more complicated alternatives under some settings, it is clear that its relative performance is strongest for small n ; the true data generating process also used a Matérn covariance function with $\nu = 5/2$,

and a visual assessment of simulation output suggests that the simple Matérn performs best when the randomly generated deformation exhibits less dramatic patterns of warping.

| | GDEF 3/2 | GDEF ∞ | S&G | Matérn 5/2 | H&H | Std. CAR |
|----------|---------------|---------------|---------------|---------------|--------|----------|
| $n = 1$ | 42.54 (0.48) | 46.66 (0.192) | - | 45.22 (0.328) | 96.06 | 76.74 |
| $n = 2$ | 28.2 (0.576) | 29.61 (0.376) | 73.6 | 42.35 (0.048) | 144.81 | 79.92 |
| $n = 3$ | 24.24 (0.6) | 24.74 (0.384) | 40.29 | 40.87 (0.016) | 77.6 | 81.14 |
| $n = 5$ | 21.93 (0.456) | 21.94 (0.536) | 32.33 (0.008) | 39.75 | 55.57 | 83.24 |
| $n = 10$ | 20.6 (0.304) | 20.4 (0.688) | 29.54 (0.008) | 39.13 | 48.4 | 83.95 |
| $n = 25$ | 19.83 (0.248) | 19.56 (0.728) | 28.53 (0.024) | 38.65 | 46.31 | 84.45 |
| $n = 50$ | 19.55 (0.24) | 19.25 (0.744) | 28.3 (0.016) | 38.36 | 45.9 | 85.08 |

Table 4: Average $KL(\Sigma, \hat{\Sigma})$ for each model and number of samples. In parentheses is the frequency across simulations that a given model produced the smallest KL divergence for a sample of size n . The GDEF models perform best across all sample sizes.

Note that the spatial deformation approach (S&G) cannot be fit for $n = 1$. This highlights one of the key advantages of our approach. Much of the literature regarding the spatial deformation framework requires that the spatial process be observed multiple times, and in some implementations requires that $n > p$. However, it is extremely common for spatial analyses to be conducted on datasets with little or no replication. Whether the deformation function is estimated using thin plate splines as in Sampson and Guttorp [1992] or a Gaussian process prior as in Schmidt and O’Hagan [2003], the inherent flexibility of the framework requires considerable amounts of data (or strong prior assumptions) to avoid over fitting. As seen in this and previous simulations, the GDEF model using the basis function representation of \mathbf{W} as presented in this paper can effectively estimate complicated patterns of spatial dependence for areal data and performs well in a setting where the true spatial process exists in continuous rather than discrete space.

4.2 Example: Mercer and Hall wheat yield data

We conclude this section with an analysis of the classic wheat yield dataset from Mercer and Hall [1911] and which is available in the spData R package. The version of the data used in the package was taken from Cressie [1993]. Mercer and Hall considered a one acre parcel of farmland that was divided into 500 rectangular plots and planted with wheat. Each plot received

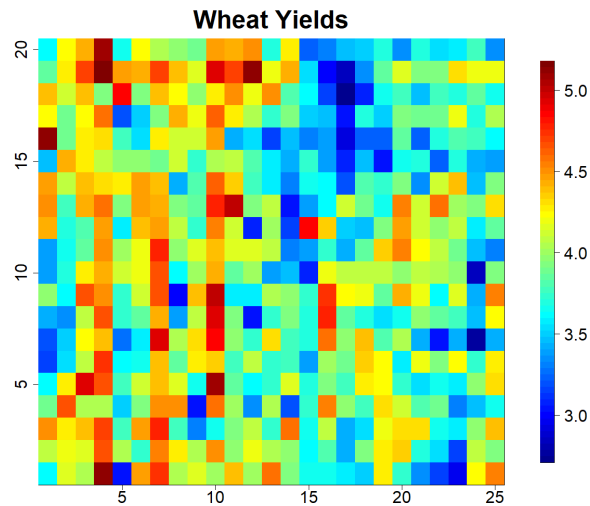


Figure 11: The Mercer Hall wheat yield data

the same treatment and soil quality was perceived to be essentially uniform at the time of planting. At harvest, the yield of each plot in pounds of grain was recorded. Figure 11 depicts the yields for each plot, which were arranged in 20 rows each containing 25 plots. Mercer and Hall discuss the variability present in the data and explore the possibility of location-based effects on yield. Noting evidence of spatial correlation, the wheat yield data was analyzed in Whittle [1954], which first introduced the simultaneous autoregressive (SAR) model, and in Besag [1974], which first introduced the CAR model. The authors of both papers found the fit of their models to the wheat yield data unsatisfactory. Looking at Figure 11, one notes that certain columns (4,7 and 10) have larger average yields than others and that within-column correlation appears to be stronger than within-row correlation. By modeling the data using fixed row and column effects Cressie [1993] found that a stationary and isotropic kriging model with plot locations given by centroids resulted in satisfactory fit, though it is worth considering whether the inclusion of row and column effects in a model for this data provide interpretive value or merely serve to improve the fit of an otherwise poorly specified model.

We propose modeling this data according to Equation 14 with the covariance of the random

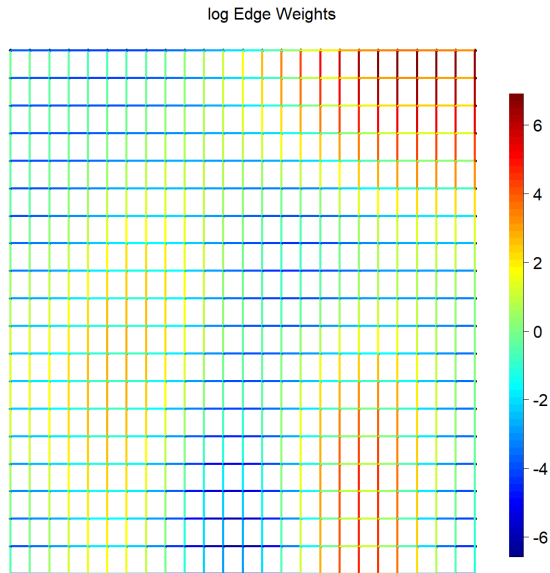


Figure 12: Estimated log edge weights

effects defined by a GDEF model with smoothness $\nu = 3/2$ and $k = 20$ basis functions. To allow for a distinction between within-column and within-row dependency, we split the intercept vector \mathbf{v}_1 of our basis into two vectors, \mathbf{v}_1^{row} and \mathbf{v}_1^{col} , where $v_{i1}^r = 1$ if edge i connects two nodes in the same row and is 0 otherwise, with \mathbf{v}_1^{col} defined similarly for columns. We obtain maximum likelihood estimates $\hat{\eta}$, $\hat{\sigma}^2$, $\hat{\tau}^2$ and $\hat{\beta}_0$ which are reported in Table 5. Negative $\hat{\eta}_1^{row}$ and positive $\hat{\eta}_1^{col}$ indicates much stronger within-column than within-row correlations. Rather than reporting the other coefficients in $\hat{\eta}$ which are individually less interpretable, Figure 12 depicts $\log(\hat{\mathbf{w}})$ over the entire network; there are three regions within the spatial domain with larger edges indicating stronger spatial correlation between nodes in those locations.

| | Est. | 95% CI |
|----------------|--------|------------------|
| η_1^{row} | -2.195 | (-3.551, -0.838) |
| η_1^{col} | 1.308 | (0.286, 2.329) |
| σ^2 | 0.146 | (0.101, 0.191) |
| τ^2 | 0.073 | (0.027, 0.118) |
| β_0 | 3.949 | (3.871, 4.026) |

Table 5: MLEs and confidence intervals for model parameters.

We can also obtain an estimate of \mathbf{z} , which may be thought of as the smoothed or “de-noised”

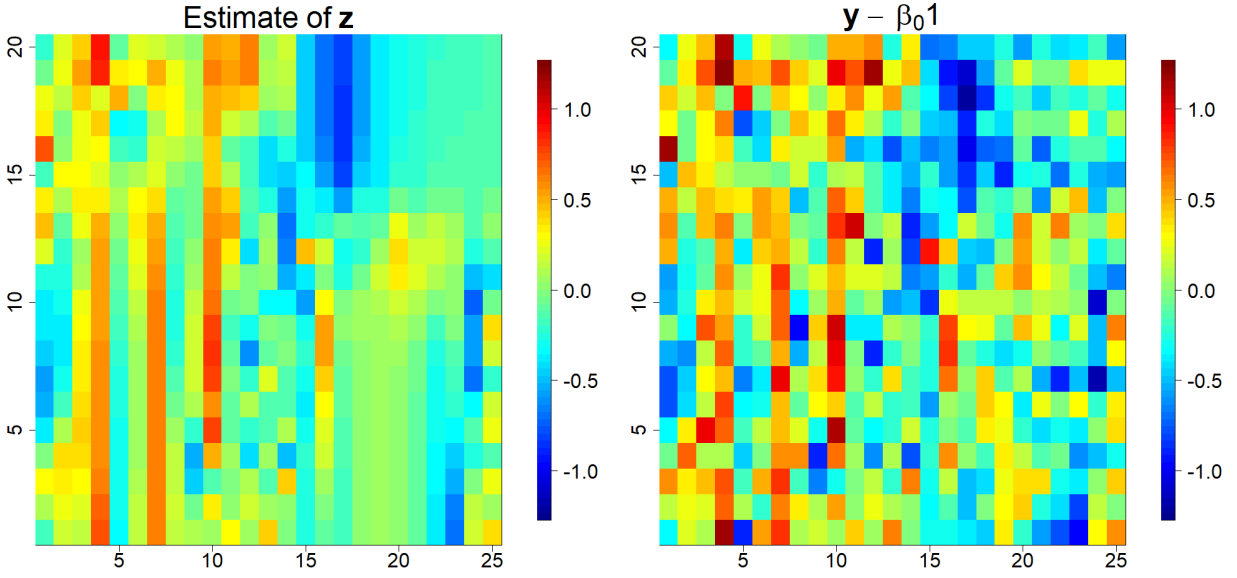


Figure 13: Estimate of \mathbf{z} (left) which acts as a smoothed version of the centered data (right)

version of the centered data. Because \mathbf{y} and \mathbf{z} are each normally distributed, the conditional distribution of \mathbf{z} is straightforward to obtain:

$$\mathbf{z}|\mathbf{y} \sim N_p \left(\left(\Phi^{-1}/\sigma^2 + \mathbf{I}_p/\tau^2 \right)^{-1} (\mathbf{y} - \beta_0 \mathbf{1})/\tau^2, \left(\Phi^{-1}/\sigma^2 + \mathbf{I}_p/\tau^2 \right)^{-1} \right). \quad (17)$$

We define $\hat{\mathbf{z}} = \left(\hat{\Phi}^{-1}/\hat{\sigma}^2 + \mathbf{I}_p/\hat{\tau}^2 \right)^{-1} (\mathbf{y} - \hat{\beta}_0 \mathbf{1})/\hat{\tau}^2$ and provide a plot of $\hat{\mathbf{z}}$ in Figure 13 alongside $\mathbf{y} - \hat{\beta}_0 \mathbf{1}$. Moran's I [Moran, 1950] is a test statistic indicating the presence or absence of spatial autocorrelation. Moran's I for the residuals of our model $\varepsilon = \mathbf{y} - \hat{\beta}_0 \mathbf{1} - \hat{\mathbf{z}}$ is 0.022, with a p-value of 0.469, indicating a lack of spatial correlation in ε . The Shapiro-Wilk normality test [Shapiro and Wilk, 1965] on the residuals results in a p-value of 0.262 indicating that the normality assumption for ε is not violated. We find that the GDEF model fits the wheat yield data well, effectively representing the distinctive and irregular patterns of spatial dependence (seen especially in the columns of the data) in an uncontrived manner.

5 Discussion

Within this article we introduced a framework for estimating edge weight matrices using the eigenvectors of the line graph’s Laplacian matrix. We show that this method may be used to enhance existing covariance models for areal data. We compared and contrasted the classically-used CAR model with the GDEF model introduced by Christensen and Hoff [2024], illustrating how both may be improved by this new framework. We evaluated properties of this method in a series of simulations and data examples. In general we find that the GDEF model is more flexible and capable of representing covariance structures with properties that are generally preferred by researchers, and that the introduced framework significantly improves the computational efficiency of the GDEF approach. We conclude this article with a brief discussion of potential avenues for future work and model extensions.

We are currently working on the development of an R package which may be used to easily implement our methodology. We also wish to evaluate how the INLA computing framework [Rue et al., 2009] may be used to complement or improve upon the model fitting approaches utilized within this article.

Part of our assessment that the GDEF model exhibits more desirable behavior than the CAR model stems from findings that the latter characterizes fundamentally non-smooth spatial processes. Rue and Held [2005] and Lindgren et al. [2011] demonstrate that it is possible to define Markov random fields (MRFs) that approximate smooth spatial processes by allowing some edge weights to be negative. The space of non-CAR MRFs is worth exploring due to their computational advantages. It may be possible to adapt our method for edge weight estimation to allow for the inclusion of negative weights in sparse precision matrix formulations, though additional work would be necessary to ensure that a valid covariance matrix is always produced.

While we have discussed estimation of \mathbf{W} within the context of explicitly defining a covariance matrix, there are other settings in which a coherent framework for flexibly defining an edge weights matrix may be valuable. For example, resistance distance is a graph metric constructed using a

matrix of non-negative edge weights that has seen widespread use in many statistical and ecological applications [Klein and Randić, 1993, Hanks and Hooten, 2013, Dickson et al., 2019]. Even if not utilized for the purpose of defining distances or covariances between locations, an edge weights matrix may be viewed as characterizing the connectivity of different regions or entities within a network.

An additional topic we would like to explore is how our method could be used to characterize the covariance of spatial processes on manifolds or restricted spatial domains. While most spatial models were developed assuming that data are observed on some well-defined subset of \mathbb{R}^2 , there is increased interest in the development of methods that can be applied to more complex domains in which Euclidean distances between observations do not accurately represent proximity with respect to the domain's underlying geometry [Yang and Dunson, 2016]. Mathematical distinctions exist between settings in which data are observed in Euclidean space but concentrated near a lower-dimensional manifold such as the surface of a sphere and settings in which an n -dimensional spatial process exists only on an irregular subset of \mathbb{R}^n due to underlying physical constraints [Dunson et al., 2022]. Sangalli et al. [2013] provides an example of the latter setting in which population density on the Island of Montréal is modeled using a spatial process which is undefined beyond island borders and within the boundaries of an airport and industrial park. Whether data is observed on a true manifold or a restricted domain, we could define a graph based on the set of observed locations, defining edges between locations based on neighbors within a small radius or through use of the Delauney triangulation [Hjelle and Dæhlen, 2006]. The LGL eigenvectors of this graph could then be utilized as in this article to define a valid covariance model over the complex spatial domain; furthermore, the flexibility of our edge weight estimation approach would ultimately allow covariance to be nonstationary with respect to the domain's underlying geometry. Some model extensions would be required in order to allow covariance to be defined continuously between observations, as our present framework is defined only at the nodes of a graph. Insight from Lindgren et al. [2011] and Lee and Haran [2022] provide potential frameworks for solving

this issue.

References

- Michael F. Christensen and Peter D. Hoff. A flexible and interpretable spatial covariance model for data on graphs. *arXiv*, 2024.
- Ephraim M. Hanks and Mevin B. Hooten. Circuit theory and model-based inference for landscape connectivity. *Journal of the American Statistical Association*, 108(501):22–33, 2013.
- Giuseppe Arbia. *Spatial data configuration in statistical analysis of regional economic and related problems*, volume 14. Springer Science & Business Media, 2012.
- Xiaoping Jin, Bradley P Carlin, and Sudipto Banerjee. Generalized hierarchical multivariate car models for areal data. *Biometrics*, 61(4):950–961, 2005.
- Catherine L Garner and Stephen W Raudenbush. Neighborhood effects on educational attainment: A multilevel analysis. *Sociology of education*, pages 251–262, 1991.
- Noel Cressie. *Statistics for spatial data*. John Wiley & Sons, 1993.
- Julian Besag. Spatial interaction and the statistical analysis of lattice systems. *Journal of the Royal Statistical Society: Series B (Methodological)*, 36(2):192–225, 1974.
- Jay M. Ver Hoef, Erin E. Peterson, Mevin B. Hooten, Ephraim M. Hanks, and Marie-Josée Fortin. Spatial autoregressive models for statistical inference from ecological data. *Ecological Monographs*, 88(1):36–59, 2018.
- Julian Besag and Charles Kooperberg. On conditional and intrinsic autoregressions. *Biometrika*, 82(4):733–746, 1995.
- Julian Besag, Jeremy York, and Annie Mollié. Bayesian image restoration with two applications in spatial statistics. *Annals of the institute of statistical mathematics*, 43(1):1–20, 1991.

- Peter Guttorp, Wendy Meiring, and Paul D. Sampson. A space-time analysis of ground-level ozone data. *Environmetrics*, 5(3):241–254, 1994.
- Bertil Matérn. Spatial variation - stochastic models and their applications to some problems in forest survey sampling investigations. *Report of the Forest Research Institute of Sweden*, 1960.
- Bedilu A. Ejigu and Eshetu Wencheke. Introducing covariate dependent weighting matrices in fitting autoregressive models and measuring spatio-environmental autocorrelation. *Spatial Statistics*, 38:100454, 2020.
- David Higdon. A process-convolution approach to modelling temperatures in the north atlantic ocean. *Environmental and Ecological Statistics*, 5:173–190, 1998.
- Sudipto Banerjee, Alan E Gelfand, Andrew O Finley, and Huiyan Sang. Gaussian predictive process models for large spatial data sets. *Journal of the Royal Statistical Society Series B: Statistical Methodology*, 70(4):825–848, 2008.
- Laura M Sangalli, James O Ramsay, and Timothy O Ramsay. Spatial spline regression models. *Journal of the Royal Statistical Society Series B: Statistical Methodology*, 75(4):681–703, 2013.
- Finn Lindgren, Håvard Rue, and Johan Lindström. An explicit link between gaussian fields and gaussian markov random fields: the stochastic partial differential equation approach. *Journal of the Royal Statistical Society Series B: Statistical Methodology*, 73(4):423–498, 2011.
- John Hughes and Murali Haran. Dimension reduction and alleviation of confounding for spatial generalized linear mixed models. *Journal of the Royal Statistical Society: Series B (Statistical Methodology)*, 75(1):139–159, 2013.
- Dave Higdon, James Gattiker, Brian Williams, and Maria Rightley. Computer model calibration using high-dimensional output. *Journal of the American Statistical Association*, 103(482):570–583, 2008.

- Ben Seiyon Lee and Murali Haran. Picar: An efficient extendable approach for fitting hierarchical spatial models. *Technometrics*, 64(2):187–198, 2022.
- Alan E Gelfand, Li Zhu, and Bradley P Carlin. On the change of support problem for spatio-temporal data. *Biostatistics*, 2(1):31–45, 2001.
- Alexandra M. Schmidt and Peter Guttorp. Flexible spatial covariance functions. *Spatial Statistics*, 37:100416, 2020.
- Michael L Stein. Limitations on low rank approximations for covariance matrices of spatial data. *Spatial Statistics*, 8:1–19, 2014.
- Abhirup Datta, Sudipto Banerjee, Andrew O Finley, and Alan E Gelfand. Hierarchical nearest-neighbor gaussian process models for large geostatistical datasets. *Journal of the American Statistical Association*, 111(514):800–812, 2016.
- Sudipto Banerjee, Andrew O Finley, Patrik Waldmann, and Tore Ericsson. Hierarchical spatial process models for multiple traits in large genetic trials. *Journal of the American Statistical Association*, 105(490):506–521, 2010.
- Daniel Spielman. Spectral graph theory. *Combinatorial scientific computing*, 18:18, 2012.
- Robert B. Gramacy and Daniel W. Apley. Local gaussian process approximation for large computer experiments. *Journal of Computational and Graphical Statistics*, 24(2):561–578, 2015.
- Matthias Katzfuss and Joseph Guinness. A general framework for bechhia approximations of gaussian processes. *Statistical Science*, 36(1):124–141, 2021.
- Joseph Guinness. Permutation and grouping methods for sharpening gaussian process approximations. *Technometrics*, 60(4):415–429, 2018.
- Julian Besag and Debashis Mondal. First-order intrinsic autoregressions and the de wijs process. *Biometrika*, 92(4):909–920, 2005.

- Christopher J Paciorek. Spatial models for point and areal data using markov random fields on a fine grid. *Electron. J. Statist.*, 7:946–972, 2013.
- Paul D. Sampson and Peter Guttorp. Nonparametric estimation of nonstationary spatial covariance structure. *Journal of the American Statistical Association*, 87(417):108–119, 1992.
- Christopher J Paciorek and Mark J Schervish. Spatial modelling using a new class of nonstationary covariance functions. *Environmetrics: The official journal of the International Environmetrics Society*, 17(5):483–506, 2006.
- Brian J Reich, James S Hodges, and Vesna Zadnik. Effects of residual smoothing on the posterior of the fixed effects in disease-mapping models. *Biometrics*, 62(4):1197–1206, 2006.
- Dale L Zimmerman and Jay M Ver Hoef. On deconfounding spatial confounding in linear models. *The American Statistician*, 76(2):159–167, 2022.
- Andrew Gelman, Jessica Hwang, and Aki Vehtari. Understanding predictive information criteria for bayesian models. *Statistics and computing*, 24(6):997–1016, 2014.
- Ben Youngman. *deform: Spatial Deformation and Dimension Expansion Gaussian Processes*, 2023. URL <https://CRAN.R-project.org/package=deform>. R package version 1.0.0.
- Alexandra M. Schmidt and Anthony O’Hagan. Bayesian inference for nonstationary spatial covariance structures via spatial deformations. *Journal of the Royal Statistical Society: Series B (Statistical Methodology)*, 65(3):743–758, 2003.
- WB Mercer and AD Hall. The experimental error of field trials. *The Journal of Agricultural Science*, 4(2):107–132, 1911.
- Peter Whittle. On stationary processes in the plane. *Biometrika*, pages 434–449, 1954.
- Patrick AP Moran. Notes on continuous stochastic phenomena. *Biometrika*, 37(1/2):17–23, 1950.

- Samuel Sanford Shapiro and Martin B Wilk. An analysis of variance test for normality (complete samples). *Biometrika*, 52(3-4):591–611, 1965.
- Håvard Rue, Sara Martino, and Nicolas Chopin. Approximate bayesian inference for latent gaussian models by using integrated nested laplace approximations. *Journal of the Royal Statistical Society Series B: Statistical Methodology*, 71(2):319–392, 2009.
- Havard Rue and Leonhard Held. *Gaussian Markov random fields: theory and applications*. Chapman and Hall/CRC, 2005.
- Douglas J. Klein and Milan Randić. Resistance distance. *Journal of mathematical chemistry*, 12(1):81–95, 1993.
- Brett G Dickson, Christine M Albano, Ranjan Anantharaman, Paul Beier, Joe Fargione, Tabitha A Graves, Miranda E Gray, Kimberly R Hall, Josh J Lawler, Paul B Leonard, et al. Circuit-theory applications to connectivity science and conservation. *Conservation biology*, 33(2):239–249, 2019.
- Yun Yang and David B Dunson. Bayesian manifold regression. *Ann. Statist.*, 40(2), 2016.
- David B Dunson, Hau-Tieng Wu, and Nan Wu. Graph based gaussian processes on restricted domains. *Journal of the Royal Statistical Society Series B: Statistical Methodology*, 84(2):414–439, 2022.
- Øyvind Hjelle and Morten Dæhlen. *Triangulations and applications*. Springer Science & Business Media, 2006.